JOURNAL OF THERMOPHYSICS AND HEAT TRANSFER
Vol. 16, No. 2, April–June 2002

Three-Dimensional Forced Convection Flow Adjacent to Backward-Facing Step

B. F. Armaly,* A. Li,† and J. H. Nie‡
University of Missouri–Rolla, Rolla, Missouri 65409

Numerical simulations of three-dimensional laminar forced convection flow adjacent to a backward-facing step in a duct are presented for the case where the duct's aspect ratio is eight (AR = 8), its expansion ratio is two (ER = 2), and the step height S is 1.00 cm. This relatively small aspect ratio duct was selected to increase the significance of the three-dimensional flow on the heat transfer downstream from the step. The flow upstream of the step is treated as fully developed and isothermal. The duct walls are treated as adiabatic surfaces with the exception of the stepped wall that is downstream from the step that is treated as being heated with uniform heat flux. Complex three-dimensional flow develops downstream from the step with a primary recirculation flow region and a reattachment length that has a minimum in its spanwise distribution near the sidewall. A spanwise swirling flow (vortex) develops inside the primary recirculation flow region and a reverse flow region develops near the sidewall. These three-dimensional features increase in size with increasing Reynolds number. The jetlike flow that develops near the sidewall within the separating shear layer impinges on the stepped wall causing a minimum to develop in the reattachment length and a maximum to develop in the Nusselt number near the sidewall. The distributions of the three velocity components, reattachment length, friction coefficient, and Nusselt number are presented and discussed.

Nomenclature

AR	=	aspect ratio, W/S
C_f	=	friction coefficient, $2\tau_w/\rho u_0^2$
C_P	=	specific heat
ER	=	expansion ratio, $H/(H - S)$
H	=	duct height downstream from the step
h	=	duct height upstream from the step
k	=	thermal conductivity
L	=	half-width (spanwise) of the duct
Nu	=	Nusselt number, $q_w S/k(T_w - T_0)$
$\boldsymbol{n}$	=	vector outer normal to surface
p	=	pressure
q_w	=	wall heat flux, $-k\partial T/\partial y\|_{y=0}$
Re	=	Reynolds number, $2\rho u_0 h/\mu$
S	=	step height
T	=	temperature
T_0	=	inlet temperature
u	=	velocity component in the x direction
u_0	=	average inlet velocity
v	=	velocity component in the y direction
W	=	width of the duct
w	=	velocity component in the z direction
x	=	streamwise coordinate axis
x_r	=	reattachment length
y	=	transverse coordinate axis
z	=	spanwise coordinate axis
μ	=	dynamic viscosity
ρ	=	density
τ_w	=	wall shear stress, $\mu\sqrt{[(\partial u/\partial y)^2 + (\partial w/\partial y)^2]}$

Received 20 March 2000; presented as Paper NHTC 2000-12301 at the 2000 National Heat Transfer Conference, ASME, AIAA, AICHE, ANS, 20–22 August 2000; revision received 13 July 2001; accepted for publication 25 September 2001.

*Curators' Professor, Department of Mechanical and Aerospace Engineering and Engineering Mechanics.
†Graduate Student, Department of Mechanical and Aerospace Engineering and Engineering Mechanics.
‡Post Doctoral Fellow, Department of Mechanical and Aerospace Engineering and Engineering Mechanics.

Introduction

SEPARATED and reattached flow occurs in heat exchanging devices, such as electronic and power-generating equipment and dump combustors. A great deal of mixing of high- and low-energy fluid occurs in the separating and reattached flow regions, thus impacting significantly the heat transfer performance of these devices. Studies on separated flow have been conducted extensively during the past decade, and the backward-facing step geometry has received most of the attention.[1–3] This geometry is simple, yet the flow and the heat transfer through it contains most of the complexities that are encountered in other, more complex, separating flow geometries, and for that reason, it has been used in benchmark studies.[4,5]

The majority of published work on separated flow deals with the two-dimensional isothermal flow behavior, and comparatively little is published about the three-dimensional nonisothermal case. Such knowledge is critical for optimizing the performance of physical heat exchanging systems, because they are mostly three-dimensional and nonisothermal. Results on three-dimensional flow behavior started to appear in the literature in the early 1990s, when computer workstations and nonintrusive measuring techniques became more readily available. The survey by Simpson[3] highlights some of the available three-dimensional studies, and most of them deal with the isothermal flow behavior. Steinthorsson et al.,[6] Williams and Baker,[7] Ku et al.,[8] Jiang et al.,[9] Chiang and Sheu,[10,11] Goyon et al.,[12] and Destefano et al.[13] used various numerical schemes to simulate in three dimensions the isothermal flow measurements of Armaly et al.[1] These simulations brought to light some of the complicated three-dimensional flow features that develop near the sidewalls at higher Reynolds numbers in this simple and large aspect ratio geometry.[1]

Results of numerical simulations for three-dimensional laminar convection heat transfer adjacent to the backward-facing step, in ducts with large aspect ratio, have also appeared in the literature. Iwai et al.[14] reported results for a duct with an aspect ratio of 16, and Pepper and Carrington[15] reported results for a duct with an aspect ratio of 12. Because of the large aspect ratio considered in these studies, the focus was on the comparisons with the two-dimensional simulations. They illustrated, however, that even at low Reynolds number, significant three-dimensional behavior occurs near the sidewalls

in these large aspect ratio ducts. The numerical study of Iwai et al.[16] established that an aspect ratio greater than 16 is needed to maintain a small two-dimensional region near the centerline of a duct having an expansion ratio of two, at a Reynolds number of 2.5×10^2. For higher Reynolds number, the flow becomes three-dimensional throughout that duct. The scarcity of three-dimensional heat transfer results in separated and reattached flow has motivated the present study.

Governing Equations and Numerical Scheme

Laminar three-dimensional forced convection flow of air in a heated duct with a backward-facing step is numerically simulated using Cartesian coordinates, as shown in Fig. 1. The height of the duct is 0.01 m and is 0.02 m upstream and downstream of the step, respectively, and its width is 0.08 m. This geometry provides a backward-facing step height of $S = 0.01$ m, expansion ratio ER $= 2$, and an aspect ratio AR $= 8$. The origin of the coordinate system is located at the bottom corner of the step where the sidewall, the backward-facing step, and the downstream stepped wall intersect, as shown in Fig. 1. Preliminary measurements of laminar flow in a similar geometry indicate that the flow downstream from the step is symmetric relative to the center width of the duct. Because of such symmetry, the width of the computational domain is chosen as half of the actual width of the duct, $L = 0.04$ m. The streamwise length of the computational domain is chosen as 0.02 and 0.5 m upstream and downstream of the step respectively, that is, $-2 \le x/S \le 50$. This choice was made to ensure that the flow upstream of the step at $x/S = -2$ is not effected significantly by the sudden expansion at the step. Previous measurements in similar geometry[1] support the preceding observations. The choice of $x/S = 50$ was made to ensure that the flow can be treated as fully developed at that plane downstream from the step, and previous measurements in similar geometry[1] support that conclusion. The laminar steady-state Navier–Stokes equations and the boundary conditions that govern the flow and the heat transfer in this geometry can be expressed as follows.

Continuity equation:

$$\frac{\partial}{\partial x}(\rho u) + \frac{\partial}{\partial y}(\rho v) + \frac{\partial}{\partial z}(\rho w) = 0 \tag{1}$$

Momentum equations:

$$\frac{\partial}{\partial x}(\rho u^2) + \frac{\partial}{\partial y}(\rho uv) + \frac{\partial}{\partial z}(\rho uw) = -\frac{\partial p}{\partial x} + \mu\left(\frac{\partial^2 u}{\partial x^2} + \frac{\partial^2 u}{\partial y^2} + \frac{\partial^2 u}{\partial z^2}\right) \tag{2}$$

$$\frac{\partial}{\partial x}(\rho uv) + \frac{\partial}{\partial y}(\rho v^2) + \frac{\partial}{\partial z}(\rho vw) = -\frac{\partial p}{\partial y} + \mu\left(\frac{\partial^2 v}{\partial x^2} + \frac{\partial^2 v}{\partial y^2} + \frac{\partial^2 v}{\partial z^2}\right) \tag{3}$$

$$\frac{\partial}{\partial x}(\rho uw) + \frac{\partial}{\partial y}(\rho vw) + \frac{\partial}{\partial z}(\rho w^2) = -\frac{\partial p}{\partial z} + \mu\left(\frac{\partial^2 w}{\partial x^2} + \frac{\partial^2 w}{\partial y^2} + \frac{\partial^2 w}{\partial z^2}\right) \tag{4}$$

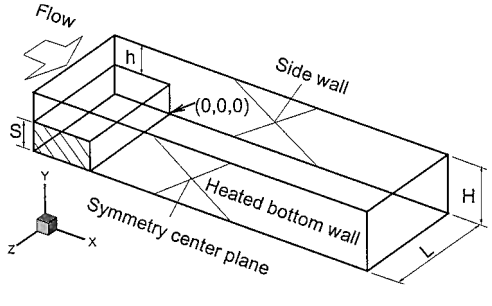

Fig. 1 Schematics of the computation domain.

Table 1 Results for four grid densities

Parameter	Grid 1	Grid 2	Grid 3	Grid 4
$x \times y \times z$	$100 \times 20 \times 20$	$125 \times 25 \times 25$	$150 \times 30 \times 30$	$180 \times 35 \times 35$
$T_{\min}$, °C	29.0	28.8	28.8	28.7
$T_{\max}$, °C	36.2	36.8	36.8	36.9
$x_{r(\text{center})}$, mm	83.4	86.7	86.4	86.5
$x_{r(\min)}$, mm	62.1	62.3	61.2	61.4

Energy equation:

$$u\frac{\partial}{\partial x}(\rho C_P T) + v\frac{\partial}{\partial y}(\rho C_P T) + w\frac{\partial}{\partial z}(\rho C_P T) = k\left(\frac{\partial^2 T}{\partial x^2} + \frac{\partial^2 T}{\partial y^2} + \frac{\partial^2 T}{\partial z^2}\right) \tag{5}$$

The physical properties are treated as constants and evaluated for air at the inlet temperature of $T_0 = 20$°C, that is, $\rho = 1.205$ kg/m^3, $\mu = 1.81 \times 10^{-5}$ kg/m·s, $k = 0.0259$ W/m·°C, and $C_p = 1.005$ kJ/kg·°C.

A no-slip boundary condition is applied at the walls. The heated stepped wall downstream from the step is maintained at uniform heat flux, $q_w = 50$W/m^2, whereas the other walls are treated as adiabatic. Fully developed flow and thermal conditions are considered at the exit section of the calculation domain, $x/S = 50$, and symmetry is applied to the center plane of the duct, $z/S = 4$. The fully developed velocities that are specified at the inlet section, $x/S = -2$, were calculated for the specified Reynolds number (isothermal flow at $T_0 = 20$°C) in a long straight duct having the same cross section and boundary conditions as the inlet section to the backward-facing step geometry. The length of that duct was 200 cm, and the inlet velocity profile was taken as uniform and equal to the average inlet velocity as calculated from the specified Reynolds number selected for that case. The exit boundary conditions were specified as fully developed, that is, $\partial u/\partial x = \partial v/\partial x = \partial w/\partial x = 0.0$. Results showed that this length is sufficient to generate fully developed flow in the duct under consideration. The fully developed velocity profiles generated from such a solution, for a specified Reynolds number flow, were used as the inlet velocity profiles at $x/S = -2$ in the solution for the backward-facing step geometry.

Numerical solution of the given governing equations and boundary conditions was performed by utilizing the commercial computational fluid dynamics (CFD) code FLUENT 5.0. The mesh is generated using FLUENT's preprocessor GAMBIT. Hexahedron volume elements were used in the simulation. At the end of each iteration, the residual sum for each of the conserved variables was computed and stored, thus recording the convergence history. The convergence criterion required that the scaled residuals be smaller than 10^{-4} for the mass and the momentum equations and smaller than 10^{-6} for the energy equation. Calculations were performed on Hewlett Packard Visualine C200 workstations, and the CPU time for converged solution for $Re = 300$ is approximately 5 h. Detailed description of the CFD code and the solution procedure may be found in the FLUENT manual.

The computational grid was generated to ensure high density at all of the walls and in the region of the step where high gradients exist, to ensure the accuracy of the simulations. Grid independence tests were performed using four grid densities and distributions for laminar forced flow at $Re = 4 \times 10^2$, and heat flux at the stepped wall equal to 21.19 W/m^2. Comparisons of results for different grid densities are presented in Table 1, and they show a difference of less than 1% between results of grid 3 and grid 4. A grid of $150 \times 30 \times 30$ downstream of the step and a grid of $20 \times 15 \times 30$ upstream of the step were selected for these simulations.

Results and Discussion

The sudden change in geometry causes flow separation at the step and flow reattachment downstream from the step. Reattachment lengths predicted by the present numerical scheme compare very favorably with other published predictions[7–9] and with measured

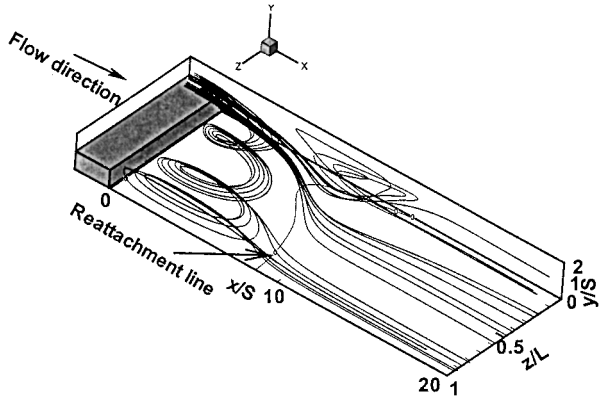

Fig. 2 Streamlines demonstrating flow features downstream from the step.

values[1] for isothermal flow in ducts having a relatively large aspect ratio, that is, two-dimensional results. Results presented in this study are limited to $Re \leq 6 \times 10^2$, where the flow remains laminar in this geometry.[1]

The negative pressure gradient that develops in the flow due to the sudden expansion at the step is responsible for developing several reverse flow regions along with swirling flow in the spanwise direction downstream from the step. The flow separates at the step and reattaches at the stepped wall forming the primary recirculation flow region. Other flow features that develop downstream from the step are shown in Fig. 2. Figure 2 shows how some streamlines (flow path of particles having zero mass) that originate from the same general region very close to the sidewall near the upper corner of the step, $x/S = 0$ and $y/S = 1$, take different paths as they flow downstream from the step. Some of these streamlines follow a counterclockwise swirling path that is increasing in size as it moves in the spanwise direction toward the center of the duct inside the primary recirculation flow region. Other streamlines that originate from the same region flow with the separating shear layer and impinge/reattach on the stepped wall. Some of these streamlines flow downstream after reattachment and others reverse their direction into the primary recirculation flow region. After reattachment, some streamlines flow toward the sidewall and upward toward the upper flat wall to form a reverse flow region near the upper corner of the sidewall. Some of that reverse flow reverses its direction again while flowing toward the center of the duct to join the downstream flow. Other portion of that reverse flow follows a clockwise swirling path (decreasing in size) in the spanwise direction toward the center of the duct.

The developments of the jetlike flow and the reverse flow region near the sidewall can be seen more clearly in Figs. 3 and 4. Streamlines are shown on a z plane that is close to the sidewall, $z/L = 0.025$, on a y plane that is close to the top wall, $y/S = 1.9$, and on a y plane that is close to the stepped wall, $y/S = 0.1$, in Figs. 3a and 3b. The streamlines in Fig. 3a show the reflected jetlike flow after reattachment as it flows toward and impinges on the upper flat wall. Part of that flow forms the sidewall reverse flow region and part continues its flow in the downstream direction. Part of the reverse flow changes its direction again to flow downstream, while another part of the reverse flow join the primary recirculation flow region. The y plane streamlines in Fig. 3a show the spanwise thickness and streamwise length of the reverse sidewall flow region, which increase as the Reynolds number increases. A jetlike flow develops within the separating shear layer as it impinges on the stepped wall, as can be seen in Fig. 3b. The streamlines in Fig. 3b show that the impingement region of the jetlike flow is in the same location as the one where the reattachment length is minimum. The dashed line that is shown in Fig. 3b is the projection of the reattachment line on that plane. Streamlines that are plotted on several z planes close to the sidewall (planes of $z/L = 0.025, 0.075, 0.15$, and 0.25) are presented in Fig. 4. The clockwise swirling flow that develops near the sidewall moves in the spanwise direction toward the upper flat wall while decreasing its size as it moves toward the center of

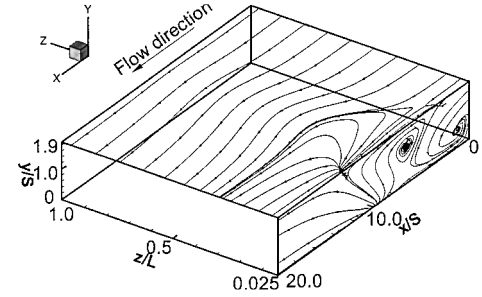

a) Adjacent to side and top walls

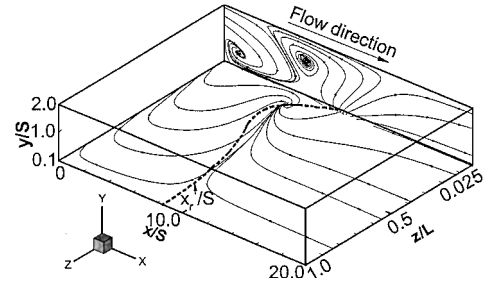

b) Adjacent to side and bottom walls, $Re = 4 \times 10^2$

Fig. 3 Streamlines demonstrating jetlike flow impingement and reverse flow regions.

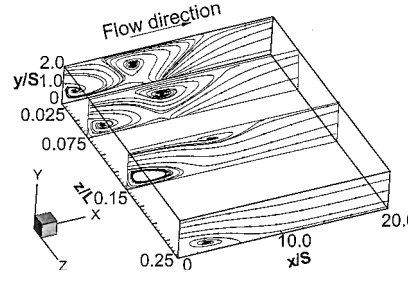

Fig. 4 Streamlines demonstrating flow on several z planes, $Re = 4 \times 10^2$.

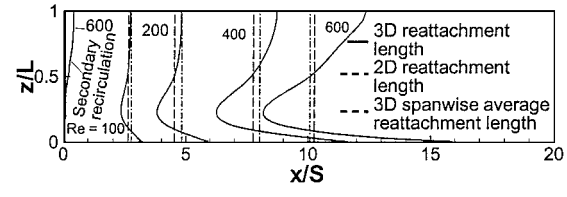

Fig. 5 Spanwise distributions of reattachment length.

the duct as seen in Fig. 4. For the conditions represented in Fig. 4, the reverse flow region that develops near the side and upper flat wall disappears for planes larger than $z/L = 0.25$.

Distributions of the primary reattachment length, x_r/S, on the stepped wall (as defined by the locations where $\partial u/\partial y|_{y=0} = 0$) are presented in Fig. 5 as a function of the spanwise coordinate z/L. The region bounded between the primary reattachment line and the step identifies the streamwise size of the primary recirculating flow region. A secondary recirculation flow region develops at the lower corner of the step and could be detected for $Re = 6 \times 10^2$. The primary and the secondary recirculating flow regions exhibit an increase in their streamwise size and a stronger spanwise variation with increasing Reynolds number. The secondary recirculation flow region has its maximum streamwise length at the center of the duct and has its minimum streamwise length at the sidewall. The streamwise length of the primary recirculation flow region (primary reattachment length) exhibits strong spanwise variations, with its maximum length occurring at the sidewall, $z/L = 0.0$, and its minimum length occurring at approximately $z/L = 0.23$. The jetlike

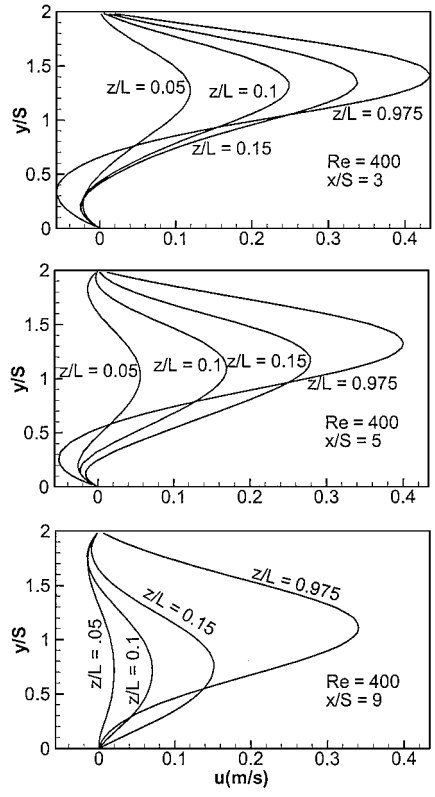

Fig. 6 Distributions of streamwise velocity component u as a function of y on different z planes.

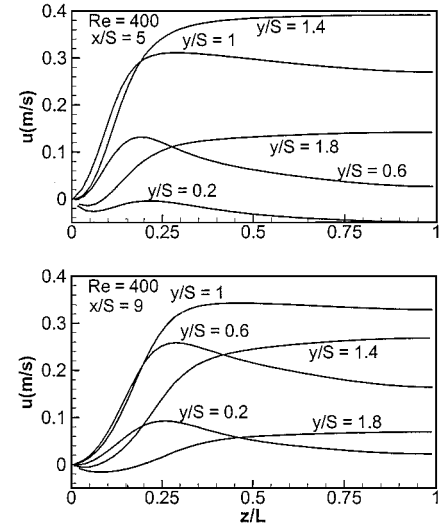

Fig. 7 Distributions of streamwise velocity component u as a function of z on different y planes.

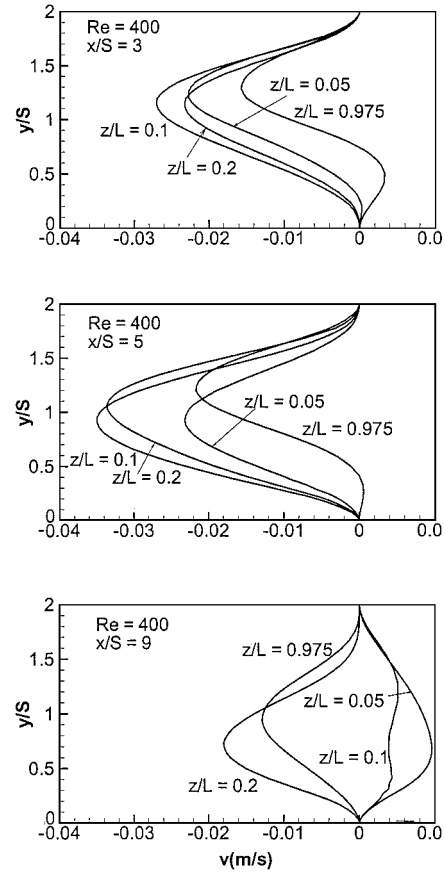

Fig. 8 Distributions of transverse velocity component v as a function of y on different z planes.

flow that develops within the separating shear layer is responsible for the minimum that develops in the primary reattachment length. The location of that minimum is the same as the jet impingement region on the stepped wall. The spanwise average of the reattachment length as determined from the three-dimensional simulations is smaller than its equivalent from two-dimensional simulations for $Re < 5 \times 10^2$, but that trend is reversed for higher Reynolds numbers, as can be seen from Fig. 5. The primary reattachment length at the center of the duct, as determined from the three-dimensional simulations, is equal to the one determined from two-dimensional simulations for a Reynolds number less than $Re = 2 \times 10^2$.

Because of space limitations, some results are presented for only one Reynolds number, but the general behavior of these results at different Reynolds numbers, $Re \leq 6 \times 10^2$, is similar to those presented for the selected Reynolds number. Transverse distributions of the streamwise velocity component u, as a function of y, on different z planes are presented in Fig. 6 at three streamwise planes x/S downstream from the step. The negative velocity values that appear in theses distributions near the wall, $y = 0$, for streamwise planes of $x/S = 3$ and 5, indicate that these planes are inside the primary recirculation flow region. By similar logic, the plane at $x/S = 9$ is downstream from the primary reattachment line. The results at $x/S = 5$ and 9 capture part of the sidewall reverse flow region that develops adjacent to the upper region of the sidewall (region close to $y/S = 2$), but that reverse flow region does not extend upstream to the plane of $x/S = 3$. In the region above the step, $y/S \geq 1$, this velocity component increases as the distance from the sidewall increases, and it decreases as the streamwise distance from the step increases. Distributions of the same velocity component as a function of z on different y planes are presented in Fig. 7 for streamwise planes of $x/S = 5$ and 9. The peak that develops in these distributions near the sidewall for planes below the step, $y/S \leq 1$, can be clearly seen in Fig. 7. Such a distribution implies that a jetlike flow is developing adjacent to the sidewall. The reverse flow region that develops near the upper wall, $y/S = 1.8$, and near to the sidewall can also be seen clearly in Fig. 7.

Distributions of the corresponding transverse velocity component v are presented in Fig. 8. These results show the general nature of the downward flow that develops as a result of the sudden expansion in the geometry. Regions with the positive values for that velocity component at $x/S = 3$ and 5 are in the primary recirculating flow region, and the one at $x/S = 9$ is in the sidewall reverse flow region. Distributions of the same velocity component are presented in Fig. 9, and they show the negative peak that develops in these distributions near the sidewall, for planes below the step, $y/S \leq 1$, resembling an impinging jetlike flow. This peak in the distribution moves away from the sidewall and toward the center of the duct as the distance from the step increases. The region with the positive velocities near the sidewall at $x/S = 9$ is part of the upward flow that develops in the sidewall swirling and reverse flow regions.

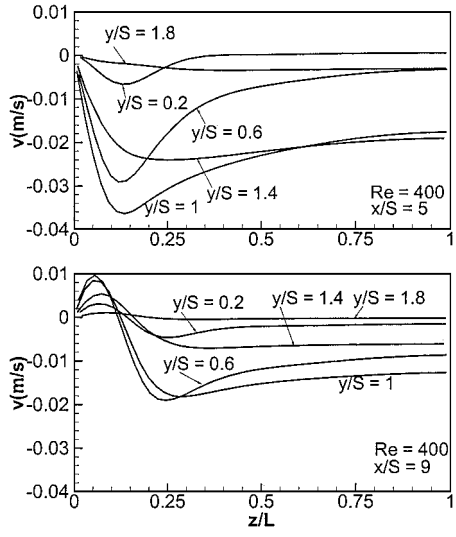

Fig. 9 Distributions of transverse velocity component v as a function of z on different y planes.

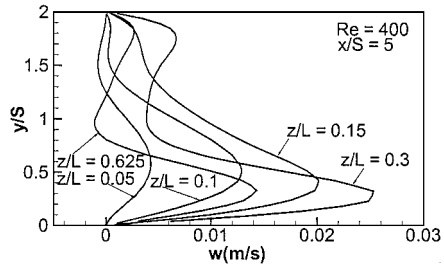

Fig. 10 Distributions of spanwise velocity component w as a function of y on different z planes.

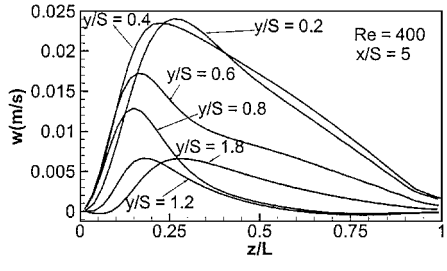

Fig. 11 Distributions of spanwise velocity component w as a function of z on different y planes.

Distributions of the corresponding spanwise velocity component w are presented in Fig. 10, and they show strong spanwise flow away from the sidewall and toward the center of the duct below the step, $y/S < 1$, and inside the primary recirculating flow region, $x/S = 5$. A peak in that velocity distribution as a function of z develops near the sidewall, as can be seen in Fig. 11, and that is similar to what has been observed for the other two velocity components. Note that, in some flow regions close to the wall, the three velocity components are of the same order of magnitude, and thus their effects on the wall shear stress and the Nusselt number cannot be neglected.

Distributions of the Nusselt number Nu on the stepped wall, $y/S = 0$, downstream from the step are presented in Fig. 12 for different Reynolds numbers. Lines of constant Nusselt numbers are plotted in Fig. 12. The dotted line in each of Fig. 12 represents the reattachment length. The maximum in the Nusselt number distribution occurs near the sidewall, and it is due to the jetlike flow that develops and impinges on that region of the wall. The maximum in the Nusselt number distribution occurs slightly downstream from the region where the reattachment length is minimum. The maximum in that distribution moves downstream from the step and closer to the

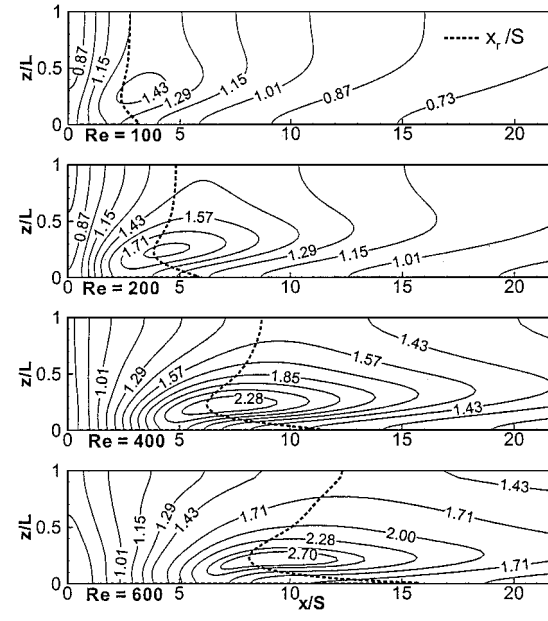

Fig. 12 Nusselt number distributions on the stepped wall, $y/S = 0$.

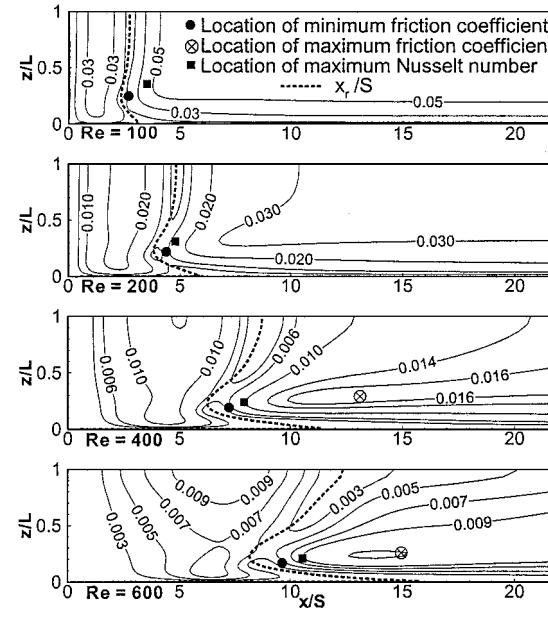

Fig. 13 Friction coefficient distributions on the stepped wall, $y/S = 0$.

sidewall as the Reynolds number increases. The maximum Nusselt number increases from 1.49 at Reynolds number of 1×10^2 to 2.84 at Reynolds number of 6×10^2. Note that the wall temperature is inversely proportional to the Nusselt number.

Distributions of the friction coefficient C_f on the stepped wall downstream from the step, $y/S = 0$, are presented in Fig. 13 for different Reynolds numbers. Lines of constant friction coefficients are plotted in Fig. 13. The dotted line on each of Fig. 13 represents the reattachment length. The wall shear stress at reattachment is not equal to zero due to the contribution of the spanwise velocity gradient to its magnitude. The minimum value of the shear stress occurs in a region close to the sidewall, and the location of that minimum moves downstream from the step and closer to the sidewall as the Reynolds number increases. The location where the maximum Nusselt number develops is downstream from the location where the minimum wall shear stress develops as identified in Fig. 13. The results for Reynolds numbers of 4×10^2 and 6×10^2 show a region where the shear stress has a maximum, and that region is near the sidewall and downstream from the location where the Nusselt

number is maximum. The results from two-dimensional simulations of the Nusselt number and the friction coefficient can be used as reasonable estimates of the spanwise average of the Nusselt number and the friction coefficient resulting from the three-dimensional flow simulations. Graphical representations of these comparisons are not presented due to space limitations.

Conclusions

Three-dimensional laminar forced convection flow adjacent to backward-facing step in a duct was numerically simulated, and the influence of the Reynolds number, in the range of $1 \times 10^2 \leq Re \leq 6 \times 10^2$, on the distributions of the Nusselt number, friction coefficient, reattachment length, and velocity distributions are reported and discussed. A jetlike flow develops in the separating shear layer adjacent to the sidewall, and its impingement on the stepped wall is responsible for the peak that develops in the Nusselt number and for the minimum that develops in the reattachment length. A swirling flow develops in the spanwise direction inside the primary recirculation flow region, and a reverse flow region develops near the sidewall. The location where the maximum Nusselt number develops for a given Reynolds number is slightly downstream from the location where the minimum shear stress develops, and both are in the region where the jetlike flow impinges on the stepped wall. The location where the Nusselt number is maximum and the shear stress is minimum for a given Reynolds number moves farther downstream and closer to the sidewall as the Reynolds number increases. The reverse flow region that develops near the sidewall extends significantly farther downstream from the step than the primary recirculating flow region. Reattachment length, Nusselt number, and shear stress obtained using two-dimensional simulations can be used as reasonable estimates for the spanwise average values obtained for these parameters using three-dimensional simulations for the range of Reynolds number examined in this study.

Acknowledgment

This work was supported in part by the National Science Foundation under Grants CTS-9906746 and CTS-9818203.

References

[1]Armaly, B. F., Durst, F., Pereira, J. C. F., and Schonung, B., "Experimental and Theoretical Investigation of Backward-Facing Step Flow," *Journal of Fluid Mechanics*, Vol. 127, 1983, pp. 473–496.

[2]Eaton, J. K., and Johnson, J. P., "A Review of Research on Subsonic Turbulent Flow Reattachment," *AIAA Journal*, Vol. 19, No. 9, 1981, pp. 1093–1100.

[3]Simpson, R. L., "Aspects of Turbulent Boundary-Layer Separation," *Progress in Aerospace Sciences*, Vol. 32, No. 5, 1996, pp. 457–521.

[4]Blackwell, B. F., and Pepper, D. W., (eds.) "Benchmark Problems for Heat Transfer Codes," HTD-Vol. 222, American Society of Mechanical Engineers, New York, 1992.

[5]Blackwell, B. F., and Armaly, B. F., (eds.) "Computational Aspects of Heat Transfer—Benchmark Problems," HTD-Vol. 258, American Society of Mechanical Engineers, New York, 1993.

[6]Steinthorsson, E., Liou, M. S., Povinelli, L. A., and Arnone, A., "Numerical Simulations of Three-Dimensional Laminar Flow over a Backward Facing Step: Flow Near Sidewalls," *Separated Flows*, edited by J. C. Button and L. P. Purtell, FED, Vol. 149, American Society of Mechanical Engineers, New York, 1993, pp. 19–26.

[7]Williams, T., and Baker, A. J., "Numerical Simulations of Laminar Flow over a 3D Backward-Facing Step," *International Journal for Numerical Methods in Fluids*, Vol. 24, No. 11, 1997, pp. 1159–1183.

[8]Ku, H. C., Hirsch, R. S., Taylor, T. D., and Rosenberg, A. P., "A Peudospectral Matrix Element Method for Solution of Three Dimensional Incompressible Flows and Its Parallel Implementation," *Journal of Computational Physics*, Vol. 83, No. 2, 1989, pp. 260–291.

[9]Jiang, B. N., Hou, L. J., and Lin, T. L., "Least-Squares Finite Element Solutions for Three-Dimensional Backward Facing Step Flow," NASA TM 106353, 1993.

[10]Chiang, T. P., and Sheu, T. W. H., "Vortical Flow over a 3-D Backward-Facing Step," *Numerical Heat Transfer, Part A–Applications*, Vol. 31, No. 2, 1997, pp. 167–192.

[11]Chiang, T. P., and Sheu, T. W. H., "A Numerical Revisit of Backward-Facing Step Flow Problem," *Physics of Fluids*, Vol. 11, No. 4, 1999, pp. 862–874.

[12]Goyon, O., Drikakis, D., and Leschziner, M. A., "Three-Dimensional Unsteady Navier–Stokes Calculations Using Hybrid Unstructured Grids," *Proceedings of 1998 ASME Fluid Engineering Division Summer Meeting*, FEDSM98-4924, American Society of Mechanical Engineers, Fairfield, NJ, 1998, pp. 1–8.

[13]Destefano, G., Denaro, F. M., and Riccardi, G., "Analysis of 3d Backward-Facing Step Incompressible Flows Via a Local Average-Based Numerical Procedure Source," *International Journal for Numerical Methods in Fluids*, Vol. 28, No. 7, 1998, pp. 1073–1084.

[14]Iwai, H., Nakabe, K., and Suzuki, K., "Numerical Simulation of Buoyancy-Assisting, Backward-Facing Step Flow and Heat Transfer in a Rectangular Duct," *Heat Transfer—Asian Research*, Vol. 28, No. 1, 1999, pp. 58–76.

[15]Pepper, D. W., and Carrington, D. B., "Convective Heat Transfer over a 3-D Backward Facing Step," *Proceedings of the ICHMT International Symposium on Advances in Computational Heat Transfer*, edited by G. de Vahl Davis and E. Leonardi, Bell House, New York, 1997, pp. 273–281.

[16]Iawi, H., Nakabe, K., and Suzuki, K., "Flow and Heat Transfer Characteristics of Backward-Facing Step Laminar Flow in Rectangular Duct," *International Journal of Heat and Mass Transfer*, Vol. 43, No. 3, 2000, pp. 457–485.